Towards in-cell structural study of light-harvesting complexes : an investigation with MAS-NMR

Azadi Chegeni, F.

CHAPTER 2

Protein & lipid dynamics in photosynthetic thylakoid membranes investigated by *in-situ* NMR

This work is published as: Azadi Chegeni F., Perin G., Sai Sankar Gupta K.B., Simionato D., Morosinotto T., Pandit A. BBA-Bioenergetics, 1857 (12): 1849-1859 (2016)

Abstract

Photosynthetic thylakoid membranes contain the protein machinery to convert sunlight into chemical energy and regulate this process in changing environmental conditions via interplay between lipid, protein and xanthophyll molecular constituents. This work addresses the molecular effects of zeaxanthin accumulation in thylakoid membranes, which occurs in native systems under high light conditions through the conversion of the xanthophyll violaxanthin into zeaxanthin via the so called xanthophyll cycle. We applied biosynthetic isotope labeling and ^{13}C solid-state NMR spectroscopy to simultaneously probe the conformational dynamics of protein, lipid and xanthophyll constituents of thylakoid membranes isolated from wild type (CW15) and *npq2* mutant of the green alga *Chlamydomonas reinhardtii*, that accumulates zeaxanthin constitutively. Results show differential dynamics of wild type and *npq2* thylakoid membranes. Ordered-phase lipids have reduced dynamics and mobile-phase lipids have enlarged dynamics in *npq2* membranes, together spanning a broader dynamical range than for WT. The total fraction of ordered lipids is much larger than the fraction of mobile lipids in thylakoid membrane, which explains why zeaxanthin accumulation causes overall reduction of thylakoid membrane fluidity. In addition to the ordered lipids, also the xanthophylls and a subset of protein sites in *npq2* thylakoid membranes have reduced conformational dynamics. Our work demonstrates the application of solid-state NMR spectroscopy for obtaining a microscopic picture of different membrane constituents simultaneously, inside native, heterogeneous membranes.

Introduction

Conversion of sunlight into chemical energy takes place inside photosynthetic membranes, where pigment-protein nano-machines carry out a cascade of reactions that evolve in time and space [1]. In order to safely perform the photosynthesis reactions and ensure organism fitness under fluctuating light conditions, constant membrane remodeling takes place. In excess light, feedback deregulation mechanisms induce quenching of sunlight excitations, dissipating the excess light energy as heat and creating a safety valve for the photosynthetic apparatus [2-3]. In plant and algae thylakoid membranes, photosynthesis is regulated through complex interplay between molecular conformational changes, reversible supramolecular interactions and membrane phase transitions [4]. Thylakoid membranes are densely packed with proteins that occupy ~70% of the membrane space and control the membrane phases [5]. Short-

and long-term acclimation of thylakoid membranes to light and cold stress involves reorganization of antenna-supercomplexes [4, 6-9], conversion of the xanthophyll violaxanthin (Vio) into zeaxanthin (Zea) via the xanthophyll cycle [10] and increase of lipid unsaturation by changing lipid composition [11]. Modulated by low pH, phosphorylation and the xanthophyll cycle, a part of the light-harvesting complex II (LHCII) antenna population disconnects from the Photosystem II (PSII) complexes and self-aggregates to form Chl-quenched states, which dissipate excess light [12]. The effects of xanthophyll composition on regulation and photoprotection in thylakoid membranes have been investigated in various studies. Zea is known to play a central role in photoprotection, through its participation in Non-Photochemical Quenching (NPQ) [13] but also by preventing lipid oxidative damage in the membrane [14]. The antioxidant activity of xanthophyll pigments present in membranes was indeed found to be related to their physical-chemical interaction with lipids [15] and their presence was shown to increase the penetration barrier to molecular oxygen [16]. Moreover, several *in vivo* and *in-vitro* studies have reported increased rigidity of Zea-containing membranes [14, 17], contributing to their stabilization. The precise role of Zea in NPQ is still under debate. *Chlamydomonas reinhardtii (Cr.) npq2* mutants, that have an impaired xanthophyll cycle and accumulate Zea constitutively in their thylakoid membranes, show faster fluorescence quenching upon actinic-light exposure [18-19]. Zea has been suggested to quench of excess energy by multiple mechanisms, by activating a quenched state in LHC protein complexes upon binding [20-22] but also at the membrane level, mediating the complexes interactions [23].

In this work, we explored the use of *in-situ* ^{13}C solid-state Nuclear Magnetic Resonance (NMR) on whole thylakoid membranes to gain insight in protein and lipid conformational dynamics and the effect of Zea accumulation. ^{13}C-NMR spectroscopy in conjunction with biosynthetic uniformly ^{13}C isotope labeling provides us with a unique method to simultaneously detect protein, lipid and xanthophyll molecular constituents and measure their molecular dynamics directly. We analyzed *Cr.* thylakoid membranes from wild type (WT) and from *npq2* mutant that, as already mentioned accumulates Zea in the thylakoid membranes. ^{13}C Magic Angle Spinning (MAS) NMR spectra were obtained by direct and cross polarization to separate and quantify rigid and dynamic membrane molecular components. To measure the temperature-dependent dynamical properties, spectra were collected over a temperature range from 0 to 25°C. In addition, $T_{1\rho}$ relaxation experiments were performed to further analyze protein backbone molecular dynamics. Results show differential dynamics of proteins, lipids and xanthophylls in WT and *npq2* membranes. The *npq2* membranes contain more xanthophylls and ordered-phase lipids with reduced dynamics, as well as mobile-phase lipids with enlarged dynamics, spanning a

broader dynamic range. Our study validates the application of ^{13}C solid-state NMR spectroscopy for functional screening of molecular membrane characteristics and demonstrates how Zea accumulation influences the conformational dynamics of protein and lipid constituents, affecting the functionality of biological thylakoid membranes.

Material & Methods

Chlamydomonas reinhardtii strains and growth conditions

In this work we employed *Cr.* strains CW15 and *npq2*. The first is a cell wall-less mutant [24] used as WT, while the second is affected in zeaxanthin epoxidase (ZE) activity [25]. Both strains were cultivated in Erlenmeyer flasks with liquid Tris-Acetate Phosphate (TAP) medium, at 100 rpm agitation and 21°C in a growth chamber. Continuous illumination was provided from cool-white fluorescent lamps under low (<25 μmoles photons m^{-2} s^{-1}) photosynthetically active radiation (400-700 nm). The TAP medium [26] used to grow labeled cells, was prepared using ^{13}C labeled sodium acetate (Sigma-Aldrich) and ^{15}N labeled ammonium chloride (Sigma-Aldrich). Cultures in labeled medium were set up starting from an optical density at 750 nm (OD_{750}) equal to 0.1 and cells were grown until OD_{750} = 1. Three rounds of cultivation in labeled medium were performed to ensure > 95 % labelling of the cells with ^{13}C and ^{15}N atoms.

Thylakoid isolation

Cells were harvested by 10 minutes of centrifugation at 4°C, at 3500×g and then washed twice in isolation medium A (IMA, 10mM MES pH 6.5, 2mM KCl, 5mM EDTA pH 8, 1M sorbitol). After centrifugation, cells were resuspended in cold IMA buffer with 0.5 % milk powder and 1 mM PMSF, 1 mM DNP-ε-amino-n-caproic acid and 1 mM benzamidine, and then disrupted at 4°C using an ultrasonic homogenizer (Sonic Rupter 400 – OMNI International - PBI) for 5 s, with the maximum power. Immediately after rupture, the samples were centrifuged for 15 minutes at 2500×g at 4°C to collect unbroken cells on the bottom of the tube. The latter were again resuspended in IMA buffer containing inhibitors and milk powder and treated again with the homogenizer. This step was repeated 3 times to be sure to break all the harvested cells, always collecting the supernatant containing the thylakoids. The latter was centrifuged for 15 minutes at 2500×g at 4°C, to eliminate cells debris. The supernatant was then centrifuged for 30 minutes at 40000×g at 4°C to collect the thylakoids. The

pellet, containing the thylakoids, was washed twice with isolation medium B (IMB, 10mM MES pH 6.5, 2mM KCl, 5mM EDTA pH 8) and resuspended in T3 buffer (50 mM Hepes-KOH pH 7.5, 5 mM $MgCl_2$, 50% glycerol). Immediately, thylakoids were frozen in liquid nitrogen and stored at −80°C until use. All steps were performed at 4°C and in dim light. Thylakoids total pigments were extracted with 80% acetone, and the chlorophyll concentration of the samples was determined spectrophotometrically using specific extinction coefficients [27] and the acetone spectra fitting, previously described in [28].

Gel electrophoresis

Coomassie-stained SDS-page was performed using 12.5% Tris-glycine gels as in [29]. Samples were solubilized with a solubilization buffer (4X) containing 30% glycerol, 125 mM Tris pH 6.8, 0.1 M dithiothreitol, 9% SDS and were loaded according to the same amount of membranes.

NMR sample preparation

The thylakoids suspension containing 1.5 mg of Chl (approx. 10 times more in protein content) were pelleted by ultra-centrifugation at 223000×g for 40 minutes and transferred into NMR rotor inserts.

NMR experimental setup

All the NMR spectra were collected with a Bruker Advance-III 750 (17.4T) solid state NMR spectrometer equipped with a 4 mm CP/ MAS trip-probe. Presented 2D ^{13}C–^{13}C proton driven spin diffusion NMR experiments (PDSD) were collected with 256 scans and mixing time of 25 ms at -29°C. Two-pulse phase modulation (TPPM) decoupling (2 dB) was applied during the t_1 and t_2 periods. Each Polarization Transfer ssNMR experiment was performed with 256 scans under SPINAL-64 decoupling (1.8 dB) and the frequency of the magic-angle spinning (MAS) was set to 11.6 kHz. All the ^{13}C spectra were referenced to the carbonyl signal of solid ^{13}C-tyrosine at 172.2 ppm. CP experiments were performed with the contact time of 2 ms, a recycle delay of 2 s and acquisition time (AQ) of 20 ms, $\omega_1^C/2\pi$ of 40.3 kHz and ^1H nutation frequency linearly ramped from 80 to 100 kHz. Two delays of 1.25ms and AQ time of 80ms were used in INEPT. For Direct Polarization (DP) experiments, delay time was 2s and acquisition time was set to 43 ms. Presented temperature curves are the averaged results of two independent sets of experiments. As a control, CP and DP experiments were also performed on a tri-amino acid ($^{13}C/^{15}N$ N- formyl-Met-Leu-Ple-OH (f-MLF)) using the same pulse sequences. In this case, CP signal

intensities were about four times the DP signal intensities, in line with expected enhancement from the ^{1}H and ^{13}C gyromagnetic ratio.

$T_{1\rho}$ setting

^{13}C $T_{1\rho}$ experiments were performed at 7 and 25°C. We applied SPINAL-64 heteronuclear decoupling with 1.5 dB power during the relaxation delay. To acquire the spectra after the CP MAS pulse, variable spin-lock pulses from 10 µs to 200 ms were applied. The acquisition time was 11 ms and τ_{CP} was set to 256 µs for all the experiments, except if stated otherwise. Relaxation curves were obtained by integrating the appropriate regions as a function of the relaxation delay in each experiment. The reported rates were determined by fitting the data to stretched- or double-exponentials.

Temperature calibration

Temperatures were calibrated by analyzing the ^{207}Pb NMR chemical shift of lead nitrate ($Pb(NO_3)_2$) which is the standard sample for temperature calibration in magic-angle spinning (MAS) probes. The readout temperature was regulated from -2.0 to 20.0°C within +/- 0.1 °C. Effective sample temperature as a function of read out temperature and spinning speed can be obtained as described in [30].

Results

^{13}C labeling of *Cr.* cells

Cr. strains CW15 (further referred to as WT) and *npq2* were chosen for this work and cultivated according to the following considerations. In order to be detectable through the solid-state NMR technique, cells needed to be labeled with carbon (^{13}C) and nitrogen (^{15}N) isotopes. While ^{15}N labeled ammonium chloride was the only nitrogen source in the medium, *Cr.* is a photosynthetic organism that is also able to fix CO_2 from the atmosphere to support its photoautotrophic metabolism. However, in mixotrophic conditions in presence of acetate, the latter becomes the prominent carbon source [31]. We exploited this metabolic feature for incorporating ^{13}C providing the carbon source in form of labeled sodium acetate. Cells were nevertheless exposed to a low light intensity, close to the compensation point, to maintain photosynthetic metabolism active. Also cells were cultivated in flasks, where CO_2 diffusion from the atmosphere is limited in order to further stimulate acetate assimilation from the medium [32].

Three rounds of cultivation in labeled medium were performed in these conditions with a tenfold dilution at every step. This assured the labeling of a very large majority of the molecules at the end of the cultivation.

Characterization by SDS-page analysis and by ^{13}C-^{13}C NMR

NMR spectra contain a wealth of structural information because the NMR isotropic chemical shifts are unique fingerprints for each type of atom. However, going from isolated protein or lipid systems to heterogeneous biological membranes, spectra become very crowded and individual molecular components are no longer resolved. Thylakoid membranes have the advantage that one type of proteins, the photosynthetic light-harvesting complexes, are abundant, reminiscent of recombinant-expressed proteins in host cell membranes. This is illustrated in figure 1, presenting a Coomassie-stained SDS-page analysis of the *Cr*. thylakoid membrane preparations of both WT and *npq2*, loaded with equal volume amounts of membrane material. The LHCII (indicated with the arrows) appears as the most abundant polypeptides in both strains. The *Cr*. LHCII trimeric complexes are isomers built from polypeptides encoded by 9 genes [33-34] with molecular masses between 22 and 26 kDa.

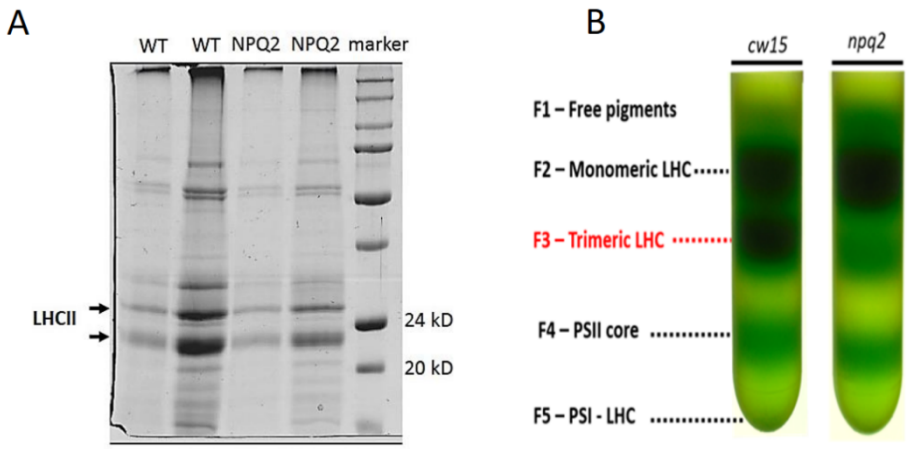

Figure 1. **A:** Coomassie-stained SDS-page of WT and *npq2 Cr*. thylakoid membranes, with 2 µl (lane 1 and 3) or 10 µl (lane 2 and 4) loading of membrane material. **B:** Monomeric and trimeric distribution of LHCII in WT and *npq2* thylakoid membranes.

Figure 2 shows a spin-diffusion ^{13}C-^{13}C NMR spectrum (PDSD, mixing time 25 ms) of the WT and *npq2* thylakoid membranes compared with the one of isolated *Cr*. LHCII. The NMR spectrum of WT thylakoid membranes strongly overlaps

with the spectrum of isolated LHCII, indicating that the LHC signals dominate the NMR spectra of thylakoid membranes, consistent with the fact that this is the most abundant protein according to the SDS-page analysis in figure 1. Nevertheless, the membrane spectra are very congested due to the fact that cells were uniformly isotope-labeled and resonances of protein, lipid and pigment constituents are detected simultaneously.

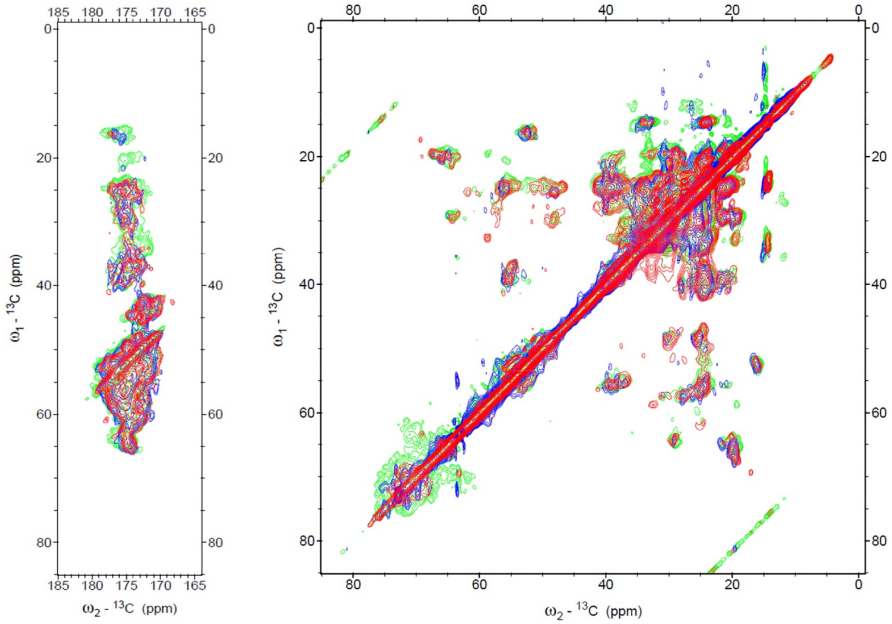

Figure 2. ^{13}C-^{13}C spectrum of isolated LHCII overlaid on the spectrum of WT and *npq2* thylakoid membranes. Green; *npq2* thylakoid membrane, red; LHCII, blue; WT thylakoid membrane.

Polarization transfer NMR

An elegant way to reduce spectral crowding and improve resolution is by use of NMR ^{1}H-^{13}C polarization-transfer spectral editing. NMR polarization-transfer experiments are selective for molecules with dynamics within a certain frequency window and filter out the NMR signals of all other components. By combining polarization-transfer experiments with different frequency filters, rigid and mobile molecular components are differentiated by their selective enhancement. In addition, the transfer of the magnetization from protons to ^{13}carbons gives rise to signal enhancement owing to the ~4 times enlarged gyromagnetic ratio of ^{1}H compared to ^{13}C. A comparison of polarization-transfer obtained spectra with spectra obtained through direct ^{13}C excitation, which

detects signals within a large frequency window, provides an estimation of the rigid and mobile fractions out of the total number of molecular constituents.

To gain insight in protein and lipid molecular dynamics inside thylakoid membranes, a set of one-dimensional solid-state ^{13}C NMR experiments were employed applying ^{1}H-^{13}C polarization-transfer sequences that used cross polarization (CP) [35] or insensitive nuclei enhancement (INEPT) [36], and applying direct ^{13}C polarization (DP)[37]. In DP experiments, the ^{13}C nuclei are directly polarized during the spin-lattice relaxation process and DP detects all type of molecular constituents. CP and INEPT experiments can be applied as frequency filters [38] that are selective for slow, resp. fast molecular dynamics. CP experiments provide NMR spectra of ^{13}C in solids or insoluble proteins by polarization transfer from ^{1}H nuclei via dipolar couplings. CP signal intensity enhancement depends on the relative gyromagnetic ratios of ^{1}H and ^{13}C, which are γ_H= 267.5 (10^6 rad S^{-1} T^{-1}) and γ_C= 67.2 (10^6 rad S^{-1} T^{-1}). The enhancement factor of the CP signal intensity compared to DP is maximal γ_H/γ_C, which is almost a factor of 4. However, the actual enhancement factor depends on molecular motions since the CP technique is based on dipolar ^{1}H-^{13}C couplings, which for dynamic molecules will average to zero, marking loss of CP signal intensity and lower CP/DP intensity ratios. Mobile constituents, on the other hand, are signal enhanced when the polarization is transferred via scalar couplings (*J*- couplings), which occur in INEPT. The process of polarization via *J*-couplings is in itself not affected by motions, but scalar coupling occurs in the transverse plane where polarization relaxation (T_2) depends on motion. Consequently, rigid segments that have fast relaxation times in the transverse plane are not detectable in INEPT [39].

In solid-state NMR spectra of bio-membranes, CP-enhanced signals typically include lipid molecules with high segmental order in the crystalline phase. Because of their restricted motions, the ^{1}H-^{13}C dipolar couplings are not averaged to zero, making CP efficient, while fast T_2 relaxation excludes their visibility in INEPT spectra. In addition, ^{13}C carbonyl resonances of membrane-embedded proteins, which have restricted conformational dynamics, are visible in CP-based spectra. INEPT is sensitive for molecules with fast (sub-nanosecond) dynamics. For bio membranes, these typically include mobile lipids with low segmental order in the fluid gel phase, which have long T_2 relaxation times that makes INEPT efficient, while averaging of the ^{1}H-^{13}C dipolar couplings by bond re-orientation excludes them from CP spectra.

We analyzed thylakoid membrane preparations of WT and *npq2* by ^{13}C MAS NMR using DP, CP and INEPT for mobile spectral editing. In addition, as a comparison the set of experiments was performed on samples of isolated LHCII

in β-dodecyl maltoside (β-DM) detergent micelles and of LHCII aggregates, obtained by detergent removal, of which preparations have been described in detail in [40]. As presented in [40] the detergent-solubilized LHCII proteins are in a fluorescent state, mimicking the proteins under active light-harvesting conditions. The LHCII aggregates are in strongly fluorescence-quenched states, mimicking the photoprotective states of the proteins. Figure 3 illustrates which thylakoid membrane components are signal-enhanced and distinguished in the CP and INEPT experiments, as described in detail below. In the additional DP experiments, in the figure 3 depicted membrane components are detected.

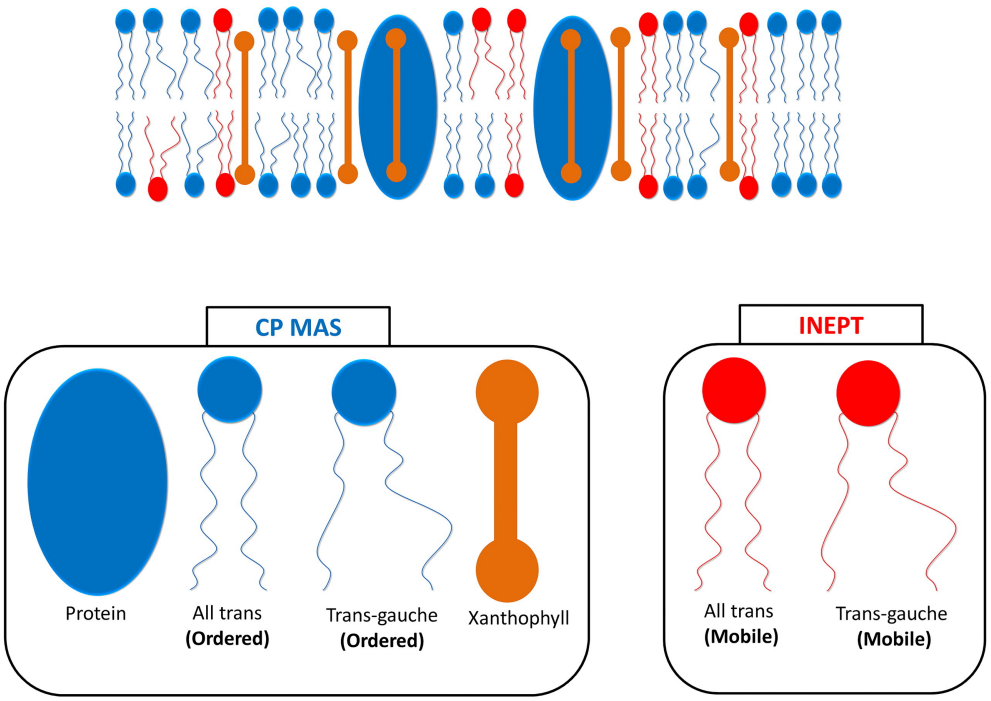

Figure 3. Illustration of thylakoid membrane constituents that are selectively probed with CP and INEPT experiments, showing the lipids in blue and red, proteins in blue and xanthophylls in orange.

Figure 4 presents the CP (blue), DP (black) and INEPT (red) ^{13}C MAS-NMR spectral intensities for WT (A) and *npq2* (B) thylakoid membranes and for WT isolated LHCII in detergent micelles (C) and LHCII aggregates (D). The INEPT spectra in figure 4 contain NMR signals characteristic for lipids, while CP spectra contain bands typical of protein backbone and side-chain carbon atoms, as well as peaks typical of fatty-acyl chains. In figure 4A and B the lipid galactosyl head-group resonances are obscured by the natural-abundance ^{13}C

resonances of glycerol that was present in the buffer. The large intensities of the lipid signals in CP (blue spectra) compared to INEPT (red spectra) indicate that the majority of the lipid molecules are in the ordered phase with restrained dynamics, while there is only a small fraction of mobile lipids. The two resonance peaks around 40 ppm are identified as Chl phytol chain signals that are visible both in CP and INEPT, and a small band between 135-140 ppm is identified as the unresolved accumulated resonances of the xanthophyll fatty-acyl chains. NMR resonances of the chlorophyll (Chl) macrocycles are not observed at ambient temperatures, but could be observed in 2D ^{13}C-^{13}C spectra at cryogenic temperatures [40].

For both the WT and *npq2* membrane preparations, protein signals from the backbone C' and C_α atoms are more pronounced in DP than in CP, indicating that the proteins have considerable conformational dynamics on micro to millisecond time scales where cross polarization becomes inefficient. As a control, CP and DP experiments were performed on a tri-peptide powder sample using the same pulse sequences (data not shown). In this case, ^{13}C CP signal intensities were roughly four times larger than the directly polarized ^{13}C signal intensities, in line with the maximal expected enhancement of CP based on the ^{1}H and ^{13}C gyromagnetic ratios for a rigid solid. For the WT, the xanthophyll band between 135-140 ppm is only observed in DP while for the *npq2* mutant the band appears in CP, indicating that *npq2* mutant contains xanthophylls with reduced fatty-acyl chain dynamics. No CP signal was detected for LHCII in β-DM micelles (figure 4C, blue curve) that undergo fast tumbling in solution, which confirms that all LHCII protein complexes were solubilized, representing a fully liquid state without protein aggregation. On the contrary, for LHCII aggregates (figure 4D), strong CP signals are detected. However, also here the DP intensities dominate over the CP, as is the case for the membrane preparations, indicating that despite their strong aggregation, the LHCII complexes possess significant dynamics on sub-millisecond time scales. The ^{13}C NMR spectra of isolated LHCII (figure 4C and D) also contain resonance signals of lipids that are co-purified with the proteins. LHCII-associated lipids are also observed in the LHCII crystal structures of *pea* and *spinach* [41-42]. In two-dimensional ^{13}C-^{13}C spin-diffusion spectra of isolated LHCII, resonances of the mono-galactosylglycerol (MGDG) and di-galactosylglycerol (DGDG) lipid sugar head groups could be resolved [40]. The 2D-resolved resonances confirm that these signals are not natural-abundance ^{13}C resonances of traces of detergent. Although galactosyl head groups of β-dodecyl maltoside detergent molecules have ^{13}C chemical shifts hat overlap with those of galactolipids, the probability of detecting natural abundance ^{13}carbons in two-dimensional ^{13}C-^{13}C spectra (~0.01%) can be neglected.

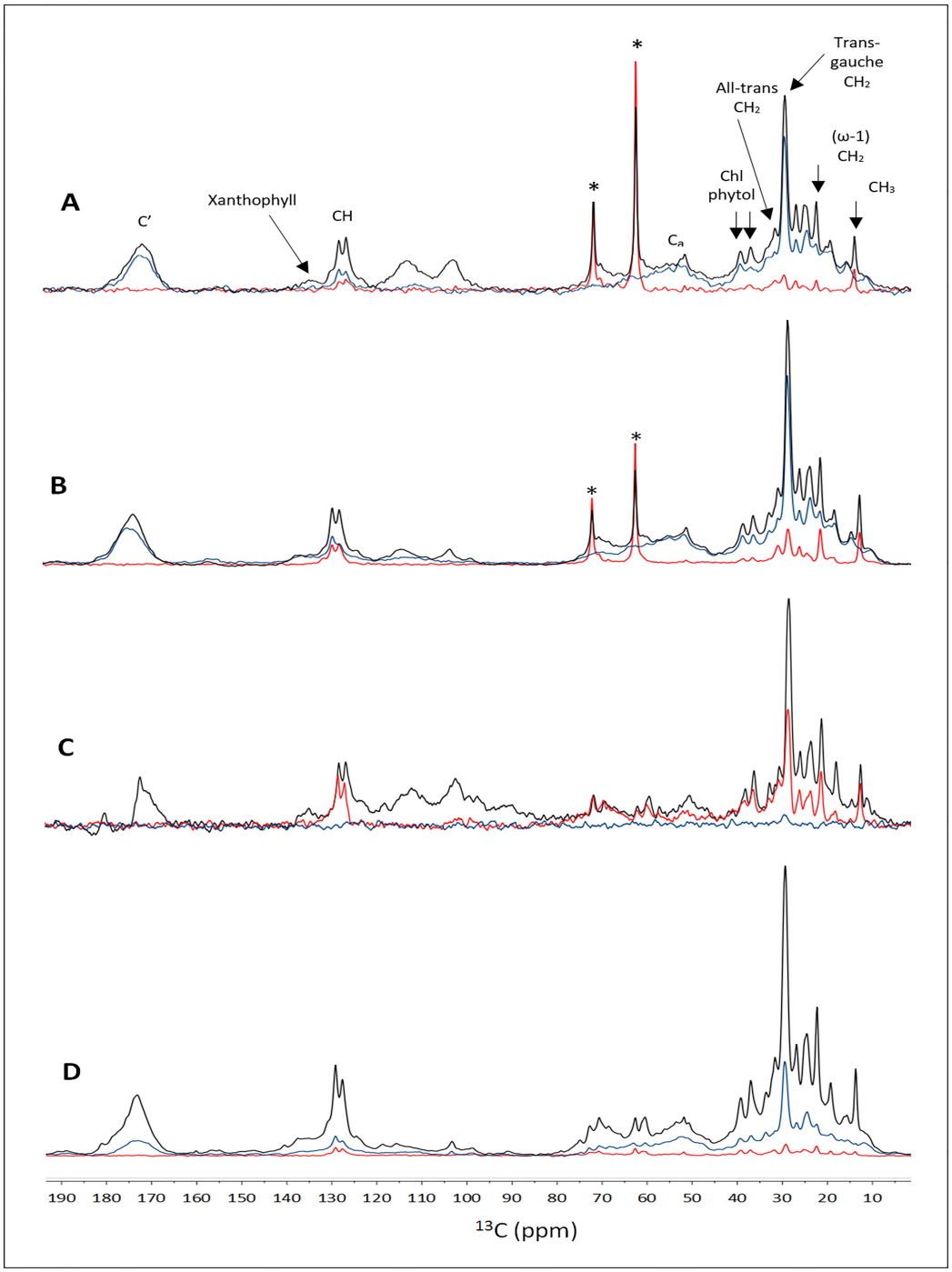

Figure 4. Overlaid ^{13}C DP (black), ^{13}C CP (blue) and ^{13}C INEPT (red) spectra recorded at 25 ^{0}C. **A:** WT thylakoid membranes; **B:** *npq2* thylakoid membranes; **C:** LHCII in detergent micelles; **D:** LHCII aggregates. *Natural-abundance ^{13}C signals of glycerol.

Temperature-dependent dynamics of protein and lipid constituents

To detect molecular dynamics over a physiological temperature range, CP and INEPT spectra were collected between 0 and 25°C. At high temperatures, a small gradual decrease of the CP intensities is observed, consistent with loss of CP efficiency due to increased molecular dynamics. This is shown in figure 5, where the carbonyl and C_α integrated peak intensities are plotted against temperature. Simultaneously, INEPT intensities, which detect the dynamic behavior of the mobile lipids, gradually increase with temperature, indicating enlargement of the fraction of mobile lipids. This is shown in the data in figure 6 that reflect the temperature-dependent dynamics of the mobile-phase lipids along their fatty-acyl chains. The end-tails of the mobile lipids are probed via the methyl (CH_3) and (ω-1) CH_2 resonances at 21 ppm (figure 6B), and their fatty-acyl chains are probed via their $n CH_2$ resonances at 30 ppm (figure 6C) and via the CH resonances between 128-132 ppm (figure 6D). The assignment of discussed resonances is presented in figure 4A and 6A. The fatty-acyl chain INEPT intensities of the *npq2* mutant increase more steeply with temperature, indicating enlarged dynamics of the mobile lipids in *npq2* membranes at elevated temperatures, compared to the WT.

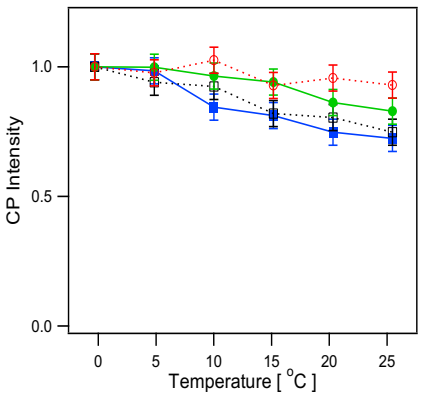

Figure 5. ^{13}C CP-MAS integrated C' and C_α intensities of WT and *npq2* as function of temperature. Filled blue squares: C' region WT; open black squares: C' region *npq2*; filled green circles: C_α region WT; open red circles: C_α region *npq*2.

The dynamics of the ordered lipids with temperature was followed in CP spectra. The lipid peaks here are not fully resolved because they overlap with the broad bands of protein side chains. Figure 7 shows the CP intensities of the main lipid peak at 30 ppm containing the unresolved $n CH_2$ resonances, and of the small

lipid peak at 32 ppm at different temperatures. Lipids can adapt an *all-trans* or *trans*-gauche conformation with different ^{13}C chemical shifts for the acyl chain carbons.

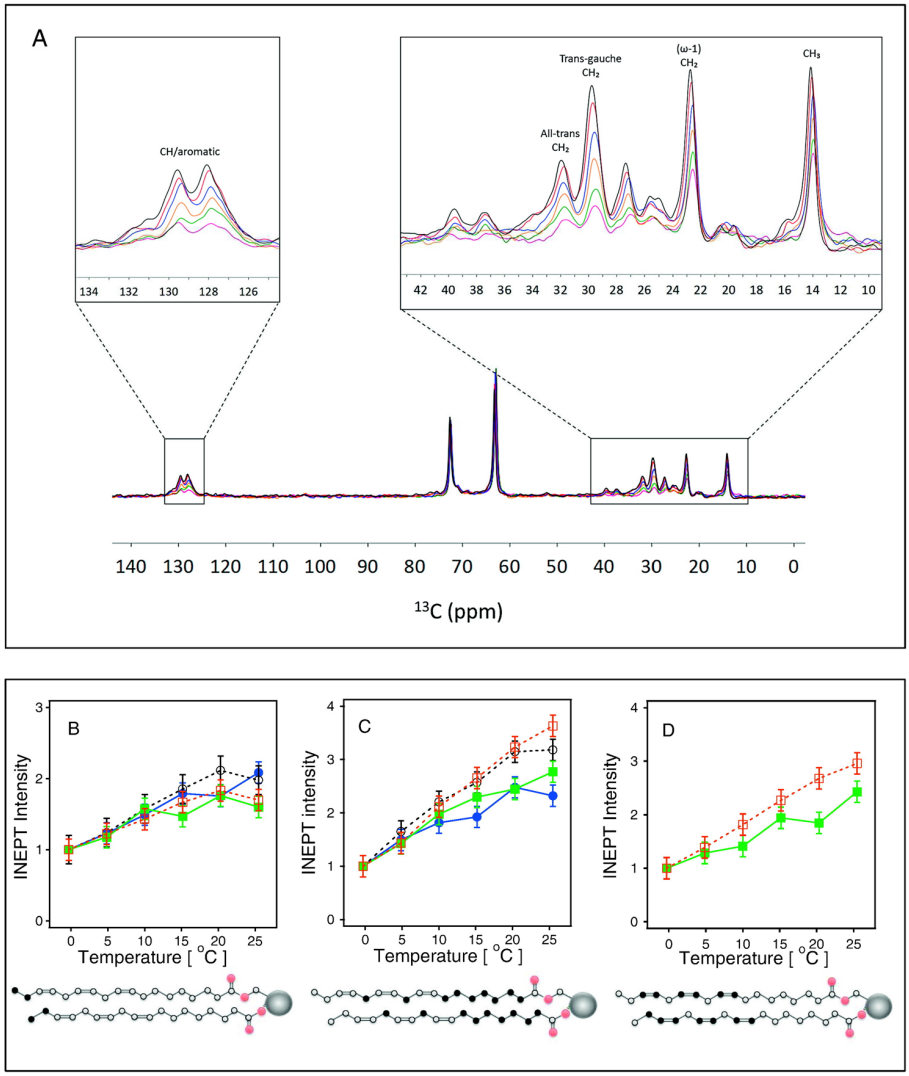

Figure 6. ^{13}C INEPT intensities of WT and *npq2* membranes at different temperatures. **A:** INEPT spectra of *npq2* recorded at temperatures between 0 and 25 °C. **B-D:** integrated INEPT spectral regions at different temperatures. The regions correspond to the lipid carbon atoms colored in black in the lipid molecules schematically drawn in the pictures below. **B:** Filled green squares: CH_3 region WT; open red squares: CH_3 region *npq2*; filled blue circles: (ω-1) CH_2 region WT; open black circles: (ω-1) CH_2 region *npq2*. **C:** Filled green squares: *trans*-gauche CH_2 region WT; open red squares: *trans*-gauche CH_2 region *npq2*; filled blue circles: *all-trans* CH_2 region WT; open black circles: *all-trans* CH_2 region *npq2*. **D:** Filled green squares: CH/aromatic region WT; open red squares: CH/aromatic region *npq2*.

The small peak at 32 ppm originates from CH_2 carbons of lipids in the *all-trans* conformation, while the main peak at 30 ppm represents the CH_2 carbons of lipids in *trans*-gauche conformation [43] (see also figures 4 and 6). The latter lipid conformation is abundant because thylakoid membranes have a high degree of unsaturated lipids. In contrast to other CP signal intensities that decrease at elevated temperatures due to enlarged molecular dynamics, the intensity of the *trans*-gauche lipid peak at 30 ppm increases with temperature. The observed increase is indicative of *all-trans* => *trans*-gauche isomerization at elevated temperatures. The gain of CP signal due to accumulation of *trans*-gauche lipids is partly compensated by loss of CP efficiency caused by increased lipid mobility. To disentangle the counteracting effects of dynamics and isomerization on the main lipid peak, we compared the 30/32 peak ratios in DP experiments that are not sensitive to dynamics changes. The WT and *npq2* membranes have similar 30/32 ratios at 7 and 25°C (0.32, resp. 0.42 for WT and 0.32, resp. 0.48 for *npq2*), from which we conclude that the fractions of *trans*-gauche and *all-trans* lipids in the two samples are similar. The differential slopes of the WT (solid lines) and *npq2* (dashed lines) temperature curves in figure 7 we therefore ascribe to differential dynamics of the ordered lipids in WT and *npq2*. The ordered lipids in *npq2* apparently are less responsive to temperature changes, with smaller losses of CP efficiencies, having reduced dynamics compared to the WT.

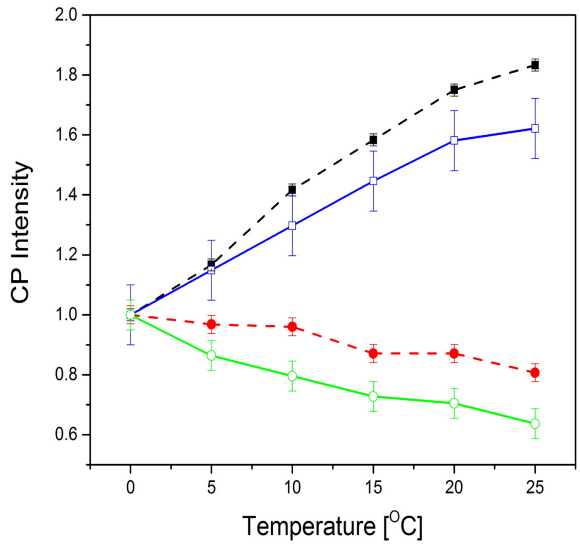

Figure 7. ^{13}C CP-MAS intensities of WT and *npq2*, illustrating lipid isomerization as a function of temperature. Filled black squares: *trans*-gauche CH_2 region *npq2*; open blue squares: *trans*-gauche CH_2 region WT; Filled red circles: *all-trans* CH_2 region *npq2*; Filled green circles: *all-trans* CH_2 region WT.

$T_{1\rho}$ relaxation experiments

In addition to the polarization-transfer experiments, we measured ^{13}C $T_{1\rho}$ relaxation of the WT and *npq2* membranes at 7 and 25 °C. Measurements of spin-lattice longitudinal relaxation in the rotating frame ($T_{1\rho}$) offer investigations of molecular dynamics from microsecond to millisecond and are sensitive to protein slow conformational dynamics. $T_{1\rho}$ describes the decay of magnetization along the RF field B_1, by applying a spin-lock pulse in the rotating frame of reference. Molecular fluctuations with frequencies close to γB_1, i.e. in the range of 10-100 kHz, will induce relaxation of the magnetization along B_1. The ^{13}C $T_{1\rho}$ relaxation rates also depend on the rate of ^{1}H-^{13}C magnetization exchange (K_{HC}) and on the ^{1}H spin-lattice relaxation rate (K_H), as illustrated in the kinetic scheme in figure 8. The mixing time during which magnetization is exchanged is set experimentally by the CP contact time, τ_{CP}.

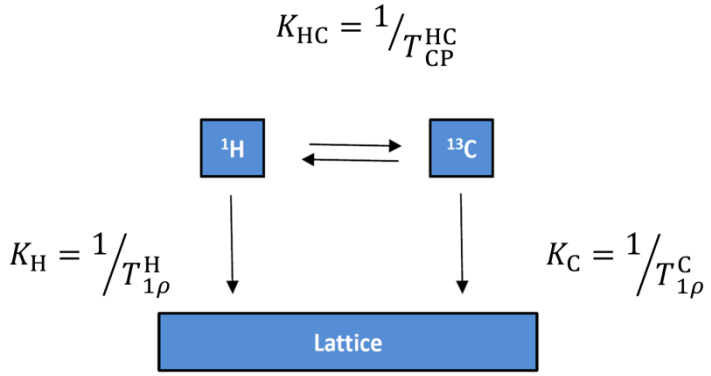

Figure 8. Kinetic scheme of ^{1}H to ^{13}C polarization transfer and $T_{1\rho}$ spin relaxation.

We performed ^{13}C $T_{1\rho}$ experiments with τ_{CP}=256 μs in order to limit proton-driven spin diffusion and inter-carbon magnetization transfer, which lead to averaging of relaxation lifetimes of neighboring carbons. Figure 9 shows the backbone $T_{1\rho}$ relaxation curves, obtained by integrating intensities over the backbone carbonyl peak. Instead of a single lifetime, we expect a distribution of lifetimes since the membranes contain a distribution of proteins and each protein contains multiple amino-acid residues with varying structures and dynamics. Therefore backbone $T_{1\rho}$ relaxation curves were fit with stretched exponentials $(e^{-t/T_{1\rho}})^{\beta}$ using a fixed parameter (β= 0.7). The C' $T_{1\rho}$ lifetimes for WT and *npq2* are similar at 7 °C, but at 25 °C the C' $T_{1\rho}$ lifetime is much more shortened for the WT, suggesting enlarged protein dynamics for the WT, but not

for *npq2* membranes, at high temperature. WT $T_{1\rho}$ relaxation curves at 7 °C were also recorded with a τ_{CP} of 2 ms. As shown in Table 1, the longer τ_{CP} shortens the observed average C' $T_{1\rho}$ from 9.4 to 6.8 ms. C_α $T_{1\rho}$ lifetimes were analyzed by taking the integrated intensities of the C_α band (see also Table 1). For some of the C_α data sets, the fit significantly improved if instead of a stretched exponential a double-exponential fit function was used, which suggests that despite the short τ_{CP} applied, the observed C_α relaxation kinetics are partly averaged over the side chains, giving rise to multi-exponential kinetics. Overall, the observed C_α lifetimes do not change much at the two temperature conditions and are quite similar for the *npq2* and WT membranes. The C_α $T_{1\rho}$ lifetimes differ significantly from the C' $T_{1\rho}$ lifetimes, confirming that the C' relaxation rates are not averaged over all the carbons, but contain the characteristics of the specific atom type.

Sample/atom	$T_{1\rho}$ (ms, 7 °C)		$T_{1\rho}$ (ms, 25 °C)	
WT				
C'	9.4 ± 1.5		1.5 ± 0.5	
C_α	± 0.3	[2.7 ± 0.9]*	± 0.4	[3.1 ± 2.0]*
C' (τ_{CP} = 2 ms)	6.8 ± 1.1		--	
npq2				
C'	10.4 ± 3.1		7.2 ± 2.2	
C_α	0.7 ± 0.5	[5.0 ± 2.0]*	0.9 ± 0.3	[4.4 ± 1.8]*
LHCII $_{agg}$				
C'	9.5 ± 4.0		1.8 ± 1.3	
C_α	0.9 ± 0.8	[3.6 ± 1.6]*	0.5	[7.9 ± 3.7]*

Table 1. $T_{1\rho}$ lifetimes of the carbonyl and C_α atoms, for WT and *npq2 Cr.* thylakoid membranes and for LHCII aggregates ($LHCII_{agg}$). *Fitting with a double-exponential fit instead of a stretched exponential; value presents the lifetimes of the slow components.

The difference between the WT and the *npq2* C' $T_{1\rho}$ lifetimes seems in apparent contradiction with the observed CP/DP ratios of the carbonyl peaks in the spectra in figure 4, that are very similar for WT and *npq2*. The reason lies in the short τ_{CP} that was used for the $T_{1\rho}$ experiments. Figure 10 shows the buildup curves for C' and C_α polarization as function of CP contact times for isolated LHCII. The rise and decay reflect the rates for resp. ^1H-^{13}C transfer, building up

the carbon magnetization, and for $T_{1\rho}$ spin-lattice relaxation as illustrated in the scheme in figure 8.

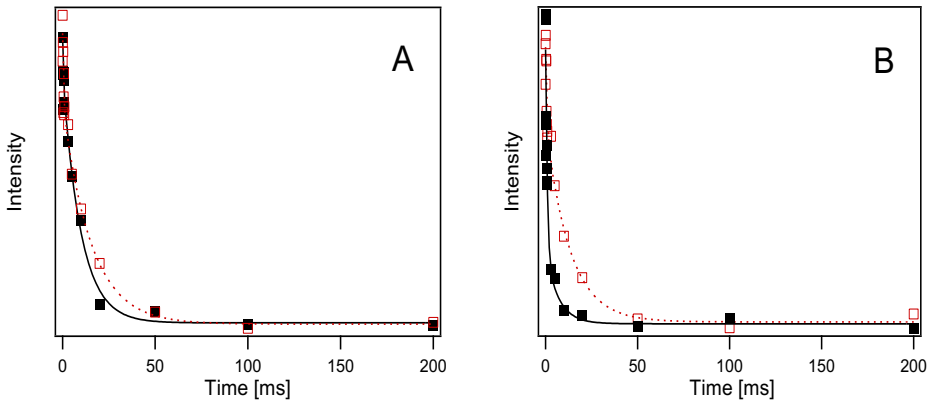

Figure 9. ^{13}C' $T_{1\rho}$ relaxation curves of WT and *npq2*. $T_{1\rho}$ relaxation at 7 °C. **A:** and 25 °C. **B:** of WT (black filled squares) and *npq2* (red open squares) and stretched-exponential fits (WT, solid black lines; *npq*2, red dashed lines). The fit relaxation lifetimes are 9.4 ms (WT, 7 °C), 10.4 ms (*npq2*, 7 °C), 1.4 ms (WT, 25 °C) and 7.8 ms (*npq2*, 25 °C).

The carbonyl carbons have slow buildup of the polarization because they lack directly attached protons. With τ_{CP}=256 µs, only a fraction of the C' carbons are polarized, while with τ_{CP}=2 ms (used for the experiments presented in figure 4) the signal is maximal and all C' carbons are polarized. As shown in Table 1, the C' $T_{1\rho}$ lifetime substantially increases with τ_{CP}=256 µs compared to τ_{CP}=2 ms. We conclude from this that with τ_{CP} = 256 µs a fraction of C' carbons is detected that has reduced conformational dynamics compared to the average carbonyls. This is consistent with the fact that dynamical molecules will have smaller ^{1}H-^{13}C coupling compare to rigid molecules, requiring longer contact times for efficient cross polarization. In contrast, the C_α carbons have a fast buildup of the polarization that is already maximal at 256 µs and have fast spin-lattice relaxation, causing loss of signal with longer τ_{CP}. The C_α $T_{1\rho}$ lifetimes thus represent the mean value of all the C_α carbons. The $T_{1\rho}$ data enables us to identify a fraction of rigid protein carbonyls that only for the WT gain significant dynamics between 7 and 25 °C.

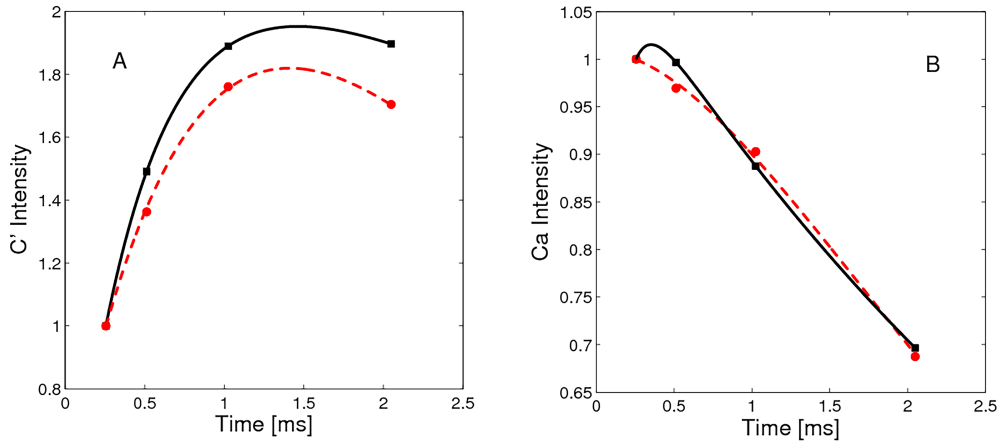

Figure 10. A: C' buildup curve of LHCII aggregates at 7 °C (black squares) and 25 °C (red circles) and double-exponential fits (7 °C, solid black lines; 25 °C, red dashed lines). B: C_α buildup curve of LHCII aggregates at 7 °C (black squares) and 25 °C: (red circles) and double-exponential fits (7 °C, solid black lines; 25 °C, red dashed lines).

Discussion

Molecular dynamics of LHCII *in-vivo* and of pigment-protein complexes *in-vitro*

Cr. thylakoid membranes are heterogeneous and contain the full photosynthetic apparatus with different protein constituents. Based on the ^{13}C-^{13}C NMR spectra that are dominated by LHCII we can conclude that the observed *in-situ* protein dynamics to large extent represent the properties of LHC proteins. Compared to the lyophilized tri-peptide model used as a control, the proteins inside thylakoid membranes contain considerable dynamics on a microsecond to millisecond time scale, reflected by the relatively low CP/DP intensity ratios. For the LHCII aggregate sample the CP/DP ratios were even lower, implying that in the aggregates the LHCII complexes retain significant mobility that is more comparable with the dynamics of polymers or hydrogels than that of protein crystals. The INEPT background signal, typical of protein C_α and side-chain atoms, could represent a small fraction of non-aggregated LHCII with high mobility. This would indicate that equilibrium exists between aggregated and free proteins, which is strongly shifted towards the aggregated forms. The lipid signals in the LHCII aggregate spectra are much more pronounced in CP than in INEPT, demonstrating that the contained lipids have restrained dynamics and likely are protein associated, and not co-purified from the bulk. No

significant CP signal could be detected for LHCII in detergent micelles at ambient temperatures, confirming that highly concentrated samples, as required for solid-state NMR, can be prepared without aggregation. Previous data have shown that CP-based spectra can be obtained of frozen protein-micelle solutions at cryogenic temperatures [40, 44-45].

The LHCII Chl macrocycle signals are neither detected by CP nor by INEPT-based ^{13}C-^{13}C spectra at ambient temperatures. Their molecular motions apparently occur on intermediate time scales where both type of experiments are inefficient. The Chl macrocycle NMR resonances of the membrane preparations emerge in NMR spectra at cryogenic temperatures and are weakly visible at 244K (data not shown). In our previous work, a dynamic transition was revealed between 223K and 244K for the Chls in detergent-solubilized LHCII [40] and their macrocycle chemical shifts started to disappear from CP-based ^{13}C-^{13}C spectra above 223K. In line with these NMR observations, quasi-elastic neutron scattering experiments showed a dynamical transition at 244K for LHCII in detergent micelles [46]. The transition was accompanied with a shift of the Chl *a* absorption maximum that was ascribed to a variety of conformational sub-states of Chl612, based on altered results for a Chl612 mutant. Our previous NMR study also showed that for LHCII aggregates the Chl macrocycle chemical shifts are still visible at 244K, demonstrating that LHCII aggregation reduces the Chl conformational dynamics. According to our low-temperature data of the thylakoid membrane samples, the conformational dynamics of protein-bound Chls in the membranes is intermediate between the values for LHCII aggregates and for LHCII detergent micelles. The difference in dynamics suggests that the detergent micelle forms an artificial microenvironment where the LHC pigment-protein complexes are more flexible than in their native states. Liposomal membranes or lipid nano-discs may provide a microenvironment that is closer to their *in-vivo* states [44, 47] and it will be of interest to address the dynamics and conformational sub-states of Chls in membrane-reconstituted LHCII.

Differential dynamics in *npq2* and WT membranes: the effects of Zea accumulation

No abrupt changes were detected following CP and INEPT intensities over the range 0-25 ^{o}C that would clearly mark a phase transition. Instead, the temperature curves show gradual increase in dynamics of the 'fast' and 'slow' membrane components and of lipid isomerization, consistent with an overall rise of membrane molecular dynamics at elevated temperatures on both fast (ps-ns) and slow (>ms) time scales. In *npq2* membranes, the ordered lipids are less sensitive to temperature changes, whereas the mobile lipids have enlarged

dynamics compared to the WT. This effect is the opposite of the reported influence of polar xanthophylls that were shown to act as membrane modulators, increasing membrane fluidity in the ordered phase, while decreasing the fluidity in the liquid crystalline phase, thereby broadening gel-to-fluid phase transitions [48]. The reverse effect might show for Zea-accumulating membranes, compared to WT membranes that mainly constitute Vio, because Zea is a less-polar xanthophyll [20]. Our lipid dynamics analysis predicts that Zea-accumulating membranes will have narrower gel-to-fluid phase transitions than for WT, which might be an advantage under stress conditions since this allows faster switching between the phases.

In both WT and *npq2* thylakoid membranes the fraction of mobile lipids is small compared to the fraction of ordered lipids. The overall membrane fluidity will therefore be dominated by the behavior of the ordered-phase lipids and consequently, is reduced for Zea-containing membranes. The fraction of ordered lipids could represent lipids that are associated with proteins or stabilized in between super complexes, while the mobile lipids represent the bulk lipids that are not in direct protein contact. The restricted dynamics of the majority of the lipids despite their large number of unsaturation suggests that in the tightly packed thylakoid membranes, where greater part of the surface area is protein occupied, most of the lipids are immobilized between the protein complexes.

The slow-dynamics membrane components that are observable via CP can be further separated in rigid and dynamic subsets based on $T_{1\rho}$ relaxation kinetics using short contact times. The $T_{1\rho}$ lifetimes indicate that the *npq2* membranes contain a subset of protein sites with limited conformational dynamics that only modestly respond to temperature changes between 7 and 25 ^{o}C. *Npq2* mutation was shown to not affect photosynthetic apparatus composition, nor photosystems antenna size, even in different light conditions [49]. In the *npq2* membranes, however, LHCII proteins are more prone to monomerization as shown in previous studies in *A. thaliana* [50-53] and confirmed in Figure 1. Upon monomerization though rather an increase of flexibility is expected than enlarged rigidity. In the *npq2* membranes however, protein aggregates may have formed that do not disassemble at high temperature and in which proteins have restricted conformational dynamics. On the other hand, $T_{1\rho}$ measurements on WT LHCII *in-vitro* aggregates do not show a reduced conformational dynamics compared to proteins in the WT membranes. Alternatively to aggregation, binding of Zea could alter the intrinsic dynamics of pigment-protein complexes at local sites. Such sites would form a subset of carbonyls that are rigidified compared to protein carbonyls in the WT membranes explaining the increased C' $T_{1\rho}$ of *npq2* membranes at room temperature. In that respect it is interesting that we also observe reduced conformational dynamics of the

xanthophylls in *npq2*. The molecular structure of Zea only differs from Vio, its epoxidized form, at the head group. Due to the de-epoxidized head groups, Zea xanthophylls are more hydrophobic [20], which could change their interactions with both the lipid and protein direct environments.

Conclusion

Summarizing the results from spectral editing and relaxation experiments, we can conclude that Zea accumulating membranes have (1) more rigid xanthophylls, (2) contain a subset of rigid protein sites that are less sensitive to temperature changes, and (3) contain thylakoid lipids that span a broader dynamical range with reduced fluidity of the large pool of ordered-phase lipids, and enlarged acyl-chain dynamics of the small pool of mobile lipids. Our observation that Zea-rich *npq2* membranes contain xanthophylls, protein and ordered-phase lipid constituents with lower backbone and fatty-acyl chain dynamics is consistent with the detected overall increase in membrane rigidity in Zea-containing membranes as discussed in literature, at least for what concerns *A. thaliana* [50, 54]. The co-existence of ordered and mobile lipids suggests that the thylakoid membranes of both WT and *npq2 Cr*. cells contain segregated membrane domains, which may differ in size and composition. Additional electron or atomic-force microscopy would have to be performed to address the effect of Zea accumulation on the supramolecular membrane organization, while additional NMR experiments on Zea-containing LHCII could address the effect of xanthophyll exchange on protein internal molecular dynamics.

References

1. Blankenship, R. E., *Molecular mechanisms of photosynthesis*. Second edition ed.; Wiley/Blackwell: Chichester, West Sussex, 2014; p 296.
2. Kruger, T. P.; Ilioaia, C.; Johnson, M. P.; Ruban, A. V.; Papagiannakis, E.; Horton, P.; van Grondelle, R., Controlled disorder in plant light-harvesting complex II explains its photoprotective role. *Biophys J* **2012,** *102* (11), 2669-76.
3. Cruz, J.; Avenson, T.; Kanazawa, A.; Takizawa, K.; Edwards, G.; Kramer, D., Plasticity in light reactions of photosynthesis for energy production and photoprotection. *Journal of experimental botany* **2005,** *56* (411), 395-406.
4. Kirchhoff, H., Structural changes of the thylakoid membrane network induced by high light stress in plant chloroplasts. *Philos Trans R Soc Lond B Biol Sci* **2014,** *369* (1640), 20130225.
5. Kirchhoff, H.; Mukherjee, U.; Galla, H. J., Molecular Architecture of the Thylakoid Membrane: Lipid Diffusion Space for Plastoquinone. *Biochemistry* **2002,** *41* (15), 4872-4882.

6. Kirchhoff, H.; Haase, W.; Wegner, S.; Danielsson, R.; Ackermann, R.; Albertsson, P. A., Low-light-induced formation of semicrystalline photosystem II arrays in higher plant chloroplasts. *Biochemistry* **2007,** *46* (39), 11169-76.
7. Kouřil, R.; Wientjes, E.; Bultema, J. B.; Croce, R.; Boekema, E. J., High-light vs. low-light: Effect of light acclimation on photosystem II composition and organization in Arabidopsis thaliana. *Biochimica et biophysica acta. Bioenergetics* **2013,** *1827* (3), 411-419.
8. Schneider, A. R.; Geissler, P. L., Coexistence of fluid and crystalline phases of proteins in photosynthetic membranes. *Biophys J* **2013,** *105* (5), 1161-70.
9. Betterle, N.; Ballottari, M.; Zorzan, S.; de Bianchi, S.; Cazzaniga, S.; Dall'osto, L.; Morosinotto, T.; Bassi, R., Light-induced Dissociation of an Antenna Hetero-oligomer Is Needed for Non-photochemical Quenching Induction. *Journal of biological chemistry* **2009,** *284* (22), 15255-15266.
10. Blankenship, R. E., *Molecular Mechanisms of Photosynthesis, 2nd Edition*. 2014.
11. Mullineaux, C. W.; Kirchhoff, H., Role of Lipids in the Dynamics of Thylakoid Membranes. **2009,** *30*, 283-294.
12. Ruban, A. V.; Johnson, M. P.; Duffy, C. D. P., The photoprotective molecular switch in the photosystem II antenna. *Biochimica et biophysica acta. Bioenergetics* **2012,** *1817* (1), 167-181.
13. Erickson, E.; Wakao, S.; Niyogi, K. K., Light stress and photoprotection in Chlamydomonas reinhardtii. *Plant J* **2015,** *82* (3), 449-65.
14. Havaux, M.; Dall'osto, L.; Bassi, R., Zeaxanthin has enhanced antioxidant capacity with respect to all other xanthophylls in Arabidopsis leaves and functions independent of binding to PSII antennae. *Plant Physiol* **2007,** *145* (4), 1506-20.
15. McNulty, H. P.; Byun, J.; Lockwood, S. F.; Jacob, R. F.; Mason, R. P., Differential effects of carotenoids on lipid peroxidation due to membrane interactions: X-ray diffraction analysis. *Biochim Biophys Acta* **2007,** *1768* (1), 167-74.
16. Subczynski, W. K.; Markowska, E.; Sieiewiesiuk, J., Effect of polar carotenoids on the oxygen diffusion-concentration product in lipid bilayers. An EPR spin label study *Biochimica el Biophysica Acta,* **1991,** *1068*, 68-72.
17. Jahns, P.; Latowski, D.; Strzalka, K., Mechanism and regulation of the violaxanthin cycle: The role of antenna proteins and membrane lipids. *Biochimica et Biophysica Acta (BBA) - Bioenergetics* **2009,** *1787* (1), 3-14.
18. Holub, O.; Seufferheld, M. J.; Gohlke, C.; Govindjee, G.; Heiss, J.; Clegg, R. M., Fluorescence lifetime imaging microscopy of Chlamydomonas reinhardtii: non-photochemical quenchingmutants and the effect of photosynthetic inhibitors on the slowchlorophyll fluorescence transient. *Journal of Microscopy,* **2006,** *226*, 90-120.
19. Niyogi, K. K.; Grossman, A. R.; Björkman, O., Arabidopsis mutants define a central role for the xanthophyll cycle in the regulation of photosynthetic energy conversion. *Plant Cell* **1998,** *10* (7), 1121-34.
20. Ruban, A. V.; Johnson, M. P., Xanthophylls as modulators of membrane protein function. *Archives of Biochemistry and Biophysics* **2010,** *504* (1), 78-85.
21. Holt, N. E.; Zigmantas, D.; Valkunas, L.; Li, X.-P.; Niyogi, K. K.; Fleming, G. R., Carotenoid Cation Formation and the Regulation of Photosynthetic Light Harvesting. *Science* **2005,** *307* (5708), 433-436.
22. Wilk, L.; Grunwald, M.; Liao, P.-N.; Walla, P. J.; Kühlbrandt, W., Direct interaction of the major light-harvesting complex II and PsbS in nonphotochemical quenching. *Proceedings of the National Academy of Sciences* **2013,** *110* (14), 5452-5456.
23. Xu, P.; Tian, L.; Kloz, M.; Croce, R., Molecular insights into Zeaxanthin-dependent quenching in higher plants. *Scientific Reports* **2015,** *5*, 13679.
24. CLARKE, A.; COULSON, G.; MORRIS, G. J., Relationship between Phospholipid Breakdown and Freezing
Injury in a Cell Wall-Less Mutant of Chiamydomonas reinhardii. *Plant Physiol* **1982,** *70*, 97-103.

25. Niyogi, K. K.; Bjorkman, O.; Grossman, A. R., Chlamydomonas Xanthophyll Cycle Mutants ldentified by Video Imaging of Chlorophyll Fluorescence Quenching *The Plant Cell* **1997,** *9*, 1369-1380.
26. Harris, E. H., The Chlamydomonas Sourcebook. A Comprehensive Guide to Biology and Laboratory Use. *Science* **1989,** *246*, 4936-1504.
27. Porra, R. J.; Thompson, W. A.; Kriedemann, W. A., Determination of accurate extinction coefficients and simultaneous equations for assaying chlorophylls a and b extracted with four different solvents: verification of the concentration of chlorophyll standards by atomic absorption spectroscopy *Biochimica et biophysica acta* **1989,** *975*, 384-394.
28. Croce, R.; Canino, G.; Ros, F.; Bassi, R., Chromophore Organization in the Higher-Plant Photosystem II Antenna Protein CP26. *Biochemistry* **20025,** *41* (7334-7343).
29. Laemmli, U. K., Cleavage of Structural Proteins during the Assembly of the Head of Bacteriophage T4. *Nature* **1970,** *227* (5259), 680-685.
30. Guan, X.; Stark, R. E., A general protocol for temperature calibration of MAS NMR probes at arbitrary spinning speeds. *Solid State Nucl Magn Reson* **2010,** *38* (2-3), 74-6.
31. Dent, R. M.; Sharifi, M. N.; Malnoe, A.; Haglund, C.; Calderon, R. H.; Wakao, S.; Niyogi, K. K., Large-scale insertional mutagenesis of Chlamydomonas supports phylogenomic functional prediction of photosynthetic genes and analysis of classical acetate-requiring mutants. *Plant J* **2015,** *82* (2), 337-51.
32. Singh, H.; Shukla, M. R.; Chary, K. V.; Rao, B. J., Acetate and bicarbonate assimilation and metabolite formation in Chlamydomonas reinhardtii: a 13C-NMR study. *PLoS One* **2014,** *9* (9), e106457.
33. Minagawa, J.; Takahashi, Y., Structure, function and assembly of Photosystem II and its light-harvesting proteins. *Photosynthesis Research* **2004,** *82*, 241-263.
34. Natali, A.; Croce, R., Characterization of the major light-harvesting complexes (LHCBM) of the green alga Chlamydomonas reinhardtii. *PLoS One* **2015,** *10* (2), e0119211.
35. Pines, A.; Waugh, J. S.; Gibby, M. G., Proton-Enhanced Nuclear Induction Spectroscopy - Method for High-Resolution Nmr of Dilute Spins in Solids. *Journal of Chemical Physics* **1972,** *56* (4), 1776.
36. Morris, G. A.; Freeman, R., Enhancement of nuclear magnetic resonance signals by polarization transfer. *J. Am. Chem. Soc* **1979,** *101* (3), 760–762.
37. Purusottam, R. N.; Bodenhausen, G.; Tekely, P., Quantitative one- and two-dimensional 13C spectra of microcrystalline proteins with enhanced intensity. *J Biomol NMR* **2013,** *57* (1), 11-9.
38. Arnold, A. A.; Genard, B.; Zito, F.; Tremblay, R.; Warschawski, D. E.; Marcotte, I., Identification of lipid and saccharide constituents of whole microalgal cells by (1)(3)C solid-state NMR. *Biochim Biophys Acta* **2015,** *1848* (1 Pt B), 369-77.
39. Diehl, P.; Fluck, E.; Kosfeld, R., *NMR Basic Principles and Progress / NMR Grundlagen und Fortschritte*. Springer-Verlag Berlin Heidelberg: 1971; p VIII, 144.
40. Pandit, A.; Reus, M.; Morosinotto, T.; Bassi, R.; Holzwarth, A. R.; de Groot, H. J. M., An NMR comparison of the light-harvesting complex II (LHCII) in active and photoprotective states reveals subtle changes in the chlorophyll a ground-state electronic structures. *Biochimica et biophysica acta. Bioenergetics* **2013,** *1827* (6), 738-744.
41. Liu, Z.; Yan, H.; Wang, K.; Kuang, T.; Zhang, J.; Gui, L.; An, X.; Chang, W., Crystal structure of spinach major light-harvesting complex at 2.72[thinsp]A resolution. *Nature* **2004,** *428* (6980), 287-292.
42. Standfuss, J.; Terwisscha van Scheltinga, A. C.; Lamborghini, M.; Kühlbrandt, W., Mechanisms of photoprotection and nonphotochemical quenching in pea light-harvesting complex at 2.5 Å resolution. *The EMBO Journal* **2005,** *24* (5), 919-928.
43. Purusottam, R. N.; Sénicourt, L.; Lacapère, J. J.; Tekely, P., Probing the gel to liquid-crystalline phase transition and relevant conformation changes in liposomes by

13C magic-angle spinning NMR spectroscopy. *Biochimica et Biophysica Acta (BBA) - Biomembranes* **2015,** *1848* (12), 3134-3139.
44. Pandit, A.; Morosinotto, T.; Reus, M.; Holzwarth, A. R.; Bassi, R.; de Groot, H. J. M., First solid-state NMR analysis of uniformly 13C-enriched major light-harvesting complexes from Chlamydomonas reinhardtii and identification of protein and cofactor spin clusters. *Biochimica et Biophysica Acta (BBA) - Bioenergetics* **2011,** *1807* (4), 437-443.
45. Pandit, A.; Buda, F.; van Gammeren, A. J.; Ganapathy, S.; de Groot, H. J. M., Selective Chemical Shift Assignment of Bacteriochlorophyll a in Uniformly [13C−15N]-Labeled Light-Harvesting 1 Complexes by Solid-State NMR in Ultrahigh Magnetic Field. *The Journal of Physical Chemistry B* **2010,** *114* (18), 6207-621 5.
46. Vrandecic, K.; Rätsep, M.; Wilk, L.; Rusevich, L.; Golub, M.; Reppert, M.; Irrgang, K.-D.; Kühlbrandt, W.; Pieper, J., Protein Dynamics Tunes Excited State Positions in Light-Harvesting Complex II. *The Journal of Physical Chemistry B* **2015,** *119* (10), 3920-3930.
47. Akhtar, P.; Pawlak, K.; Kovacs, L.; Bota, A.; Dorogi, M.; Kovács, L.; Bóta, A.; Kiss, T.; Garab, G.; Lambrev, P., Pigment Interactions in Light-harvesting Complex II in Different Molecular Environments. *Journal of biological chemistry* **2015,** *290* (8), 4877-4886.
48. Gruszecki, W. I.; Strzałka, K., Carotenoids as modulators of lipid membrane physical properties. *Biochimica et Biophysica Acta (BBA) - Molecular Basis of Disease* **2005,** *1740* (2), 108-115.
49. Kalituho, L.; Rech, J.; Jahns, P., The roles of specific xanthophylls in light utilization. *Planta* **2007,** *225* (2), 423-39.
50. Tardy, F.; Havaux, M., Thylakoid membrane fluidity and thermostability during the operation of the xanthophyll cycle in higher-plant chloroplasts. *Biochimica et biophysica acta* **1997,** *1330* (2), 179-93.
51. Lokstein, H.; Tian, L.; Polle, J. E. W.; Penna, D. D., Xanthophyll biosynthetic mutants of Arabidopsis thaliana: altered nonphotochemical quenching of chlorophyll £uorescence is due to changes in Photosystem II antenna size and stability. *Biochimica et Biophysica Acta* **2002,** *1553*, 309-319.
52. Havaux, M.; Dall'Osto, L.; Cuine, S.; Giuliano, G.; Bassi, R., The effect of zeaxanthin as the only xanthophyll on the structure and function of the photosynthetic apparatus in Arabidopsis thaliana. *J Biol Chem* **2004,** *279* (14), 13878-88.
53. Dall'Osto, L.; Caffarri, S.; Bassi, R., A mechanism of nonphotochemical energy dissipation, independent from PsbS, revealed by a conformational change in the antenna protein CP26. *Plant Cell* **2005,** *17* (4), 1217-32.
54. Havaux, M., Carotenoids as membrane stabilizers in chloroplasts. *Trends in Plant Science* **1998,** *3* (4), 147-151.